ACS APPLIED MATERIALS & INTERFACES

Research Article

www.acsami.org

Magnetoceramics from the Bulk Pyrolysis of Polysilazane Cross-Linked by Polyferrocenylcarbosilanes with Hyperbranched Topology

Jie Kong,*[,†] Minmin Kong,[†] Xiaofei Zhang,[†] Lixin Chen,[†] and Linan An[‡]

[†]Key Laboratory of Space Applied Physics and Chemistry of Ministry of Education, Department of Applied Chemistry, School of Science, Northwestern Polytechnical University, Xi'an 710072, P. R. China

[‡]Department of Materials Science and Engineering, Advanced Materials Processing and Analysis Center, University of Central Florida, Orlando, Florida 32816, United States

Supporting Information

ABSTRACT: In this contribution, we report a novel strategy for the synthesis of nanocrystal-containing magnetoceramics with an ultralow hysteresis loss by the pyrolysis of commercial polysilazane cross-linked with a functional metallopolymer possessing hyperbranched topology. The usage of hyperbranched polyferrocenylcarbosilane offers either enhanced ceramic yield or magnetic functionality of pyrolyzed ceramics. The ceramic yield was enhanced accompanied by a decreased evolution of hydrocarbons and NH_3 because of the cross-linking of precursors and the hyperbranched cross-linker. The nucleation of Fe_5Si_3 from the reaction of iron atoms with Si–C–N amorphous phase promoted the formation of α-Si_3N_4 and SiC crystals. After annealing at 1300 °C, stable Fe_3Si crystals were generated from the transformation of the metastable Fe_5Si_3 phase. The nanocrystal-containing ceramics showed good ferromagnetism with an ultralow (close to 0) hysteresis loss. This method is convenient for the generation of tunable functional ceramics using a commercial polymeric precursor cross-linked by a metallopolymer with a designed topology.

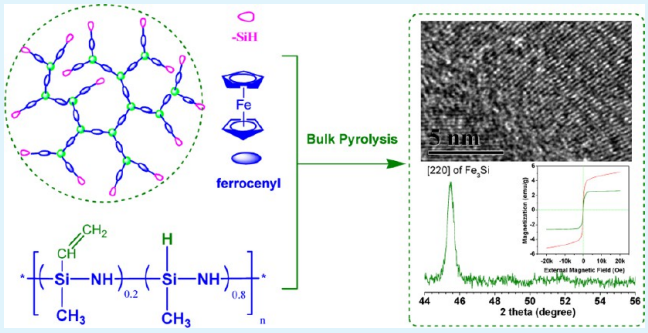

KEYWORDS: *magnetoceramics, polymeric precursors, hyperbranched, cross-linker*

1. INTRODUCTION

Polymer-derived ceramics (PDCs) have attracted remarkable interest in the last 2 decades because of their improved properties and ability to be transformed into diverse shapes, such as fibres,[1−6] highly porous components,[7−9] micro-electromechanical systems,[10−13] and Li-ion battery anodes[14−16] via liquid-phase sintering,[17] ultra-high-pressure hot isostatic pressing,[18] or spark plasma sintering[19] in comparison to conventional ceramics. Among the PDCs, transition-metal-containing Si–C–N ceramics (e.g., Co, Fe, Ni, Pd, Pt, Cu, and Au) are of special interest in engineering fields because of their interesting electrical, magnetic, and catalytic properties. The tailoring and preparation of such Si–C–N ceramics with a late transition metal at a lower temperature that have an improved control over composition, microstructure, and final form are always an advantage. The first way to prepare such ceramics is by blending the precursor with a metal or metal-oxide powder. A liquid polysilazane had been previously demonstrated to be mixed with iron or iron carbonyl,[20] Fe_3O_4,[21] $FeCl_2$,[22] $FeCl_3$,[23] $Fe(NO_3)_3$,[24] and ferrocene,[25] respectively. The subsequent pyrolysis up to 1000−1100 °C, in a nitrogen atmosphere, leads to the formation of Si–Fe–C–N magnetic materials with a potential for application in harsh environments. However, this method is limited by the particle size of the metal (oxide) powders. At the same time, a heterogeneous morphology with dispersed iron-based particle grains (α-Fe, Fe_3C, or Fe_3Si) is usually observed in the ceramic matrix because inorganic powders are insoluble with the organic precursors.[21−25]

As an alternative, a chemical modification of the polymeric precursor via coordination compounds was studied in which a metal (e.g., Fe, Co, Ni, Pt, and Cu) is transferred from the coordination compounds to the polymer chains to yield metal-enhanced PDCs.[26,27] More recently, the chemical modification of commercial polysilazane by a Ni(II) complex of trans-[bis(2-aminoetanol-*N*,*O*)diacetato-nickel(II)][28] or [Ni-(4-methyl-2-((trimethylsilyl)amino)-pyridine)$_2$]$_2$[29] has been reported for the formation of a Ni nanoparticle containing nanoporous silicon oxycarbo-nitride ceramics. Similarly, an amino-pyridinato copper complex of [Cu_2-((4-methylpyridin-2-yl)-trimethylsilanylamine)$_2$] was employed to modify polysilazane via an aminopyridine elimination reaction.[30] The cross-linking of copper-modified polysilazane and subsequent pyrolysis lead to the formation of crystalline copper-containing ceramics. The copper was reduced to copper metal during pyrolysis at 1000 °C. The so-called Cu@SiCN ceramics showed catalytic activity

Received: August 17, 2013
Accepted: September 23, 2013
Published: September 23, 2013

Table 1. Composition of Si−C−N and Si−Fe−C−N Ceramics Derived from Polymeric Precursors at 1100 °C and under an Argon Atmosphere

	precursors				atomic composition (%)[c]					
sample	hb-PolyFc (wt %)[a]	PSN (wt %)	ceramic yield (%)[b]	ceramic	Si	C	N	O[d]	Fe/Si[e]	Si−Fe−C−N formula
P0	100		15.0							
P1		100	74.6	C1	26.60	48.22	12.93	12.24		$Si_1C_{1.81}N_{0.49}$
P2	5	95	82.3	C2	27.37	40.47	16.25	15.91	0.01	$Si_1Fe_{0.01}C_{1.48}N_{0.59}$
P3	15	85	81.5	C3	26.86	43.08	15.81	14.26	0.03	$Si_1Fe_{0.03}C_{1.60}N_{0.59}$
P4	33	67	77.7	C4	23.78	52.08	11.69	12.45	0.06	$Si_1Fe_{0.06}C_{2.19}N_{0.49}$

[a]The weight-average molecular weight (M_w) and polydispersity index (PDI) are 5200 g/mol and 2.38, respectively, as determined by SEC with a PS calibration. [b]Ceramic yield was measured using TGA at 1300 °C under an argon atmosphere. [c]Atomic composition was determined using XPS. [d]The introduction of oxygen is mainly due to the absorption of the ceramic powders before the XPS measurement. [e]The ratio of silicon and iron was measured by EDX.

toward oxidation of cycloalkanes in the presence of air as an oxidant.[30]

As another convenient method, the controlled pyrolysis of metallopolymers offers several advantages including an improved control over composition, microstructure, and final form of the expected materials. One class of such representative metallopolymers are polyferrocenylsilanes (PFS) and their block copolymers,[31−33] which have been shown to have a potential in shaped magnetic ceramics[34−40] and self-assembled spheres,[41] cylinders,[42] or 1D nanostructures,[43,44] with magnetic properties that can be tuned between a ferromagnetic and superparamagnetic state. Besides the linear PFS mentioned above, a metallopolymer with a hyperbranched topology also has a possibility to be transformed into ceramics with tailored components and functionality.[38−40,45−48]

Normally, the hyperbranched metallopolymers, such as hyperbranched polyferrocenylcarbosilanes, possess numerous terminal reactive groups, such as silicon hydrogen bonds, vinyls, or alkynyl groups. Therefore, they can act as natural functional cross-linkers for the general precursors like polysilazanes, polycarbosilanes, or polyorganosilylcarbodiimides. Besides, the specific method of cross-linking of a polymer precursor has a significant influence on the local phase composition and/or the microstructural features of the resulting ceramics.[49]

For soluble hyperbranched metallopolymers, the first merit lies in the numerous termini, which can promote the cross-linking of precursors, resulting in a high ceramic yield. Second, the transition-metal atoms from hyperbranched polymers can be introduced and help in controlling the composition and magnetic or catalytic property. Third, in contrast to the insoluble inorganic metal compounds or complex coordination compounds, they can be used for obtaining a homogeneous nanostructure of the formed ceramics. In this contribution, we report a novel strategy to synthesize Si−Fe−C−N magneto-ceramics by bulk pyrolysis of commercial polysilazane cross-linked by a polyferrocenylcarbosilane with hyperbranched topology, which offers a convenient synthesis strategy for tunable magnetoceramics with a homogeneous nanostructure.

2. EXPERIMENTAL SECTION

2.1. Materials. . Ferrocene (98%), chlorodimethylsilane (98%), *N*,*N*,*N*′,*N*′-tetramethylethylenediamine (TMEDA), *n*-butyllithium (1.6 M in hexane), and platinum-1,3-divinyl-1,1,3,3-tetramethyldisiloxane complex (0.1 M in poly(dimethylsiloxane) terminated with vinyl) (Karstedt's catalyst) were purchased from Alfa Aesar China (Tianjin, China). Trivinylmethylsilane (95%) was received from Gelest Inc. Commercial polysilazane (PSZ) (The Institute of Chemistry, Beijing, China) was used as-received without any further purification. The molar ratio of the vinyl groups and silicon hydrogen bonds in the main chains is 1:4, according to the NMR integral. Anhydrous tetrahydrofuran (THF), hexane, and toluene were freshly distilled under reflux using sodium/benzophenone.

2.2. Synthesis of hb-PolyFc. The hyperbranched polyferrocenylcarbosilane terminated with silicon hydrogen bonds (hb-PolyFc) was synthesized from the A_2 monomer, 1,1′-bis(dimethylsilyl)-ferrocene, and the B_3 monomer, trivinylmethylsilane. Here, 1,1′-bis(dimethylsilyl)ferrocene was synthesized from ferrocene and chlorodimethylsilane as described previously.[50] For the synthesis of hb-PolyFc, a 100 mL flame-dried flask equipped with a Teflon stir bar and high-vacuum stopcock was charged with trivinylmethylsilane (0.74 g, 6.0 mmol), 10 mg of Karstedt's catalyst, and 25.0 mL of toluene under an argon atmosphere. Next, 1,1′-bis(dimethylsilyl)ferrocene (1.82 g, 6.0 mmol) was added dropwise into the solution at 45 °C. After 12 h, no Si−H bond resonance at 2110 cm^{-1} was observed by FTIR spectroscopy. The solvent was removed by rotary evaporation (40 mbar, 50 °C) to yield the crude product hb-PolyFc as a brown liquid. Subsequently, the crude product was dissolved in 5 mL of diethyl ether and precipitated into 50 mL of methanol three times. The precipitate was dried in a vacuum oven for 48 h (10 mbar, 60 °C). Finally, hb-PolyFc was obtained as a brown viscous liquid with a yield of 72%. The detailed information on hb-PolyFc, including the NMR spectrum, molecular weight, and degree of branching, is presented in Figures S1 and 2 and Table 1.

2.3. Preparation of Ceramics. The PSZ and hb-PolyFc were mixed under an argon atmosphere using a Schlenk tube. As shown in Table 1, for a typical sample, 0.25, 1.25, and 1.65 g of hb-PolyFc and 20 mL of anhydrous tetrahydrofuran were added to 4.75, 3.75, and 3.35 g of PSZ, respectively. The solvent was then evaporated at 60 °C under vacuum using a liquid-nitrogen trap. Three grams of the as-prepared brown liquid was transferred into the tube furnace (GSL-1700X, Kejing New Mater. Ltd., Hefei, China) for pyrolysis under an argon atmosphere. The cross-linking of the samples was performed at 200 °C (heating rate: 5 K/min, holding time: 2 h) followed by pyrolysis at 1100 °C (heating rate: 5 K/min, holding time: 4 h). After cooling to ambient temperature, a black powder product of millimeter dimensions was obtained.

2.4. Characterization. Simultaneous thermogravimetric analysis and differential scanning calorimetry coupled with mass spectrometry was performed using a simultaneous thermoanalyzer STA 449 F3 coupled with a quadrupole mass spectrometer QMS 403 C Aëolos (Netzsch Group, Germany) at a temperature range between 40 and 1400 °C, with a heating rate of 10 K/min under an argon atmosphere (gas flow: 50 mL/min).

Powder X-ray diffraction (XRD) measurement was conducted on an X'Pert Pro Powder diffractometer from PANalytical (Cu Kα radiation, 40 kV, 40 mA) (PANalytical B.V., Netherlands). The X'Celerator Scientific RTMS detection unit was used for detection.

X-ray photoelectron spectroscopy (XPS) measurements were conducted on a Kα spectrometer (Thermo Fisher Scientific, Waltham, MA, USA), and the core level spectra were measured using a monochromatic Al K R X-ray source. The analyzer was operated at a 23.5 eV pass energy, and the analyzed area was 800 μm in diameter.

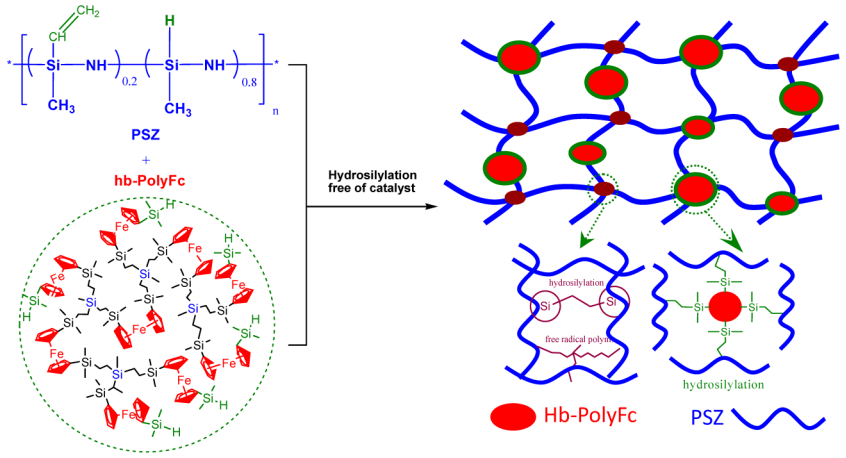

Figure 1. Schematic structure of polymeric precursors PSZ and hb-PolyFc and their cross-linked network after hydrosilylation or free-radical polymerization below 300 °C.

Binding energies were referenced to the adventitious hydrocarbon C 1s line at 285.0 eV, and the curve fitting of the XPS spectra was performed using the least-squares method.

Scanning electron microscopy (SEM) and energy-dispersive spectroscopy (EDS) analyses were performed using a VEGA3 XMH instrument (Tescan Co., Czech Republic). The sample was measured after sputtering a thin layer (1 to 2 nm) of gold. Transmission electron microscopy (TEM, FEI, Tecnai G2 F20) was operated at 200 kV, coupled with electron diffraction analysis. A 5 μL droplet of an ultrasonic dispersion mixture (0.02 g/L) of a milled sample and alcohol was dropped onto a copper grid (200 mesh) coated with a carbon film and dried at ambient temperature for 30 min.

Pore volume and surface area analysis of the selected ceramic powders were carried out by N_2 sorption isothermal analysis at −195.8 °C according to the Brunauer−Emmett−Teller (BET) method (77.350 K, TriStar II 3020, Micromeritics Instrument Co., Norcross, GA, USA). The powdered samples were degassed at 150 °C for 24 h prior to nitrogen adsorption measurements. The adsorption isotherm was used to determine the pore-size distribution via the Barret−Joyner−Halender (BJH) method.

The magnetic properties of the samples were studied using a magnetic-property measurement system (MPMS, Quantum Design Inc., San Diego, CA, USA) utilizing a superconducting quantum interference device (SQUID). Magnetic behavior was studied with a constant applied magnetic field. Furthermore, the magnetization as a function of the applied field (from −20 kOe to 20 kOe) was recorded at 25 °C.

3. RESULTS AND DISCUSSION

3.1. Pyrolysis Behavior of Polymeric Precursors. The linear PSZ was employed here because it was one of general polymeric precursors for PDCs. The molecular structure was characterized by ^{1}H NMR and SEC, as presented in Figure S1 (Supporting Information). Similar to the well-known HT1800,[29,30] the molar ratio of silicon hydrogen bonds and vinyl groups on the main chain is 4:1 with a M_n of 800 g/mol. The hb-PolyFc was prepared via the hydrosilylation of the A_2 monomer, 1,1′-bis(dimethylsilyl)ferrocene, and B_3 monomer, trivinylmethylsilane,[45] with a M_w of 5200 g/mol and a degree of branching of 0.71, as shown in Table 1 and Figures S2 and S3. The ^{1}H and ^{29}Si NMR spectra confirm the silicon hydrogen bonds with a proton resonance at 4.42 ppm and a branched structure. As is already known, PSZ can be formed as cross-linked networks via hydrosilylation or free-radical polymerization below 300 °C. The high density of hydrogen bonds on the termini makes it possible to incorporate hb-PolyFc into the cross-linked networks of PSZ by hydrosilylation in the absence of a catalyst. The schematic route followed for this study is illustrated in Figure 1.

Simultaneous thermogravimetric analysis and differential scanning calorimetry coupled with mass spectrometry was conducted to investigate the cross-linking and pyrolysis behavior of these precursor systems, as presented in Table 1. The simultaneous TGA and DSC results of PSZ (P1) and Fe-containing precursors P0, P2, P3, and P4 are presented in Figure 2. From the TGA curves, it can be observed that hb-PolyFc (P0) undergoes a rapid thermolytic degradation in the

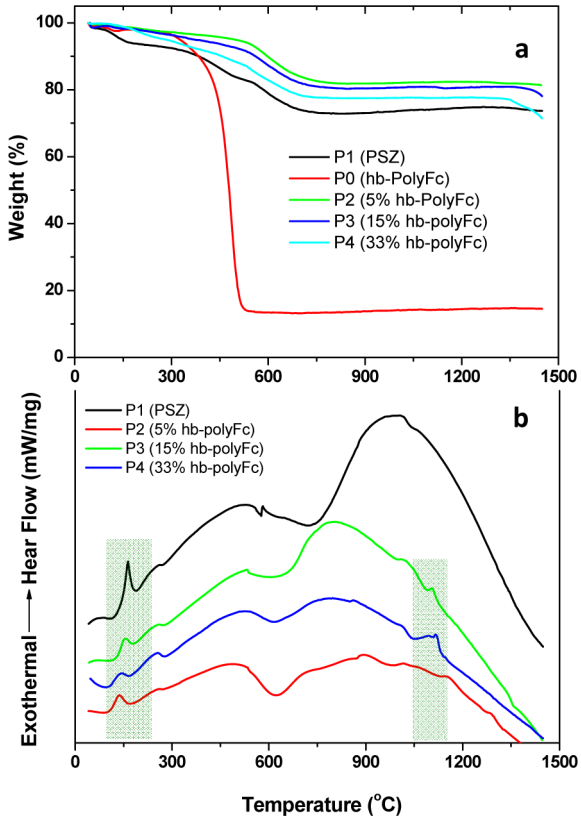

Figure 2. Polymeric precursor thermograms obtained from simultaneous thermal analysis of TGA and DSC under an argon atmosphere at a scanning rate of 10 K/min. (a) TGA curves and (b) DSC curves.

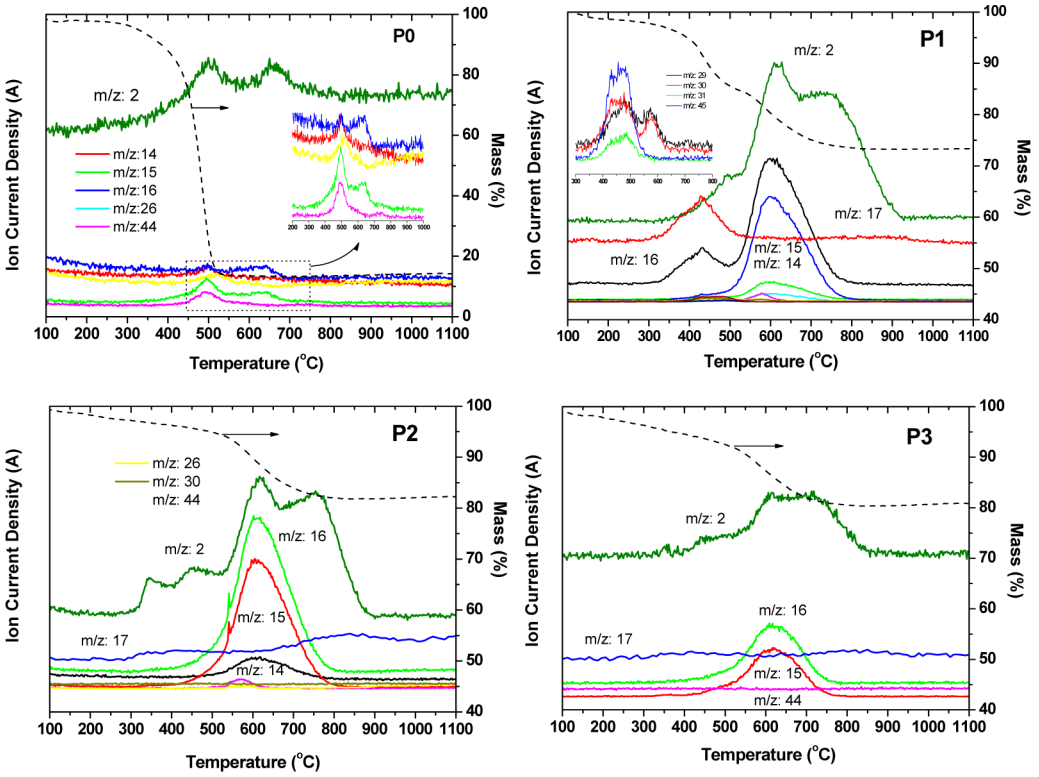

Figure 3. Thermograms of simultaneous thermogravimetry (dashed lines) and mass spectrometry analysis of the precursors P0, P1, P2, and P3 with the evolution of species (m/z = 2–45).

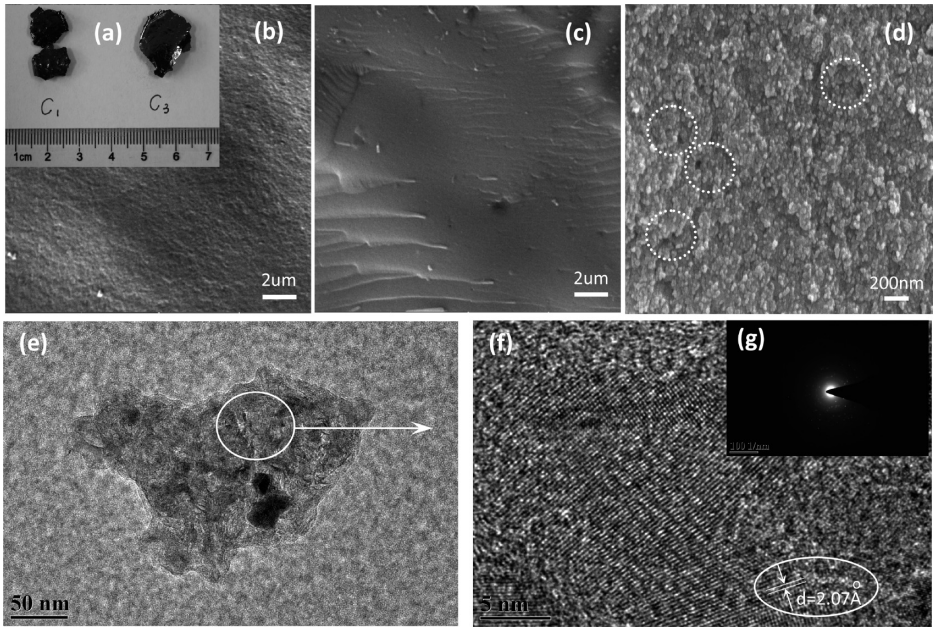

Figure 4. . Morphology of ceramics. (a) Photograph of bulk ceramics, (b) SEM image of a cross-section of C3, (c) SEM image of a cross-section of C2, (d) SEM image of a cross-section of C4, (e) TEM image of the dispersed milled ceramic of C4, (f) enlarged TEM image of C4, and (g) electron diffraction pattern.

temperature range of 300–550 °C, after which the TGA curve almost levels off. The ceramic yield under this condition is 15.0%, which is very low. However, the mixture of hb-PolyFc and PSZ (i.e., P2, P3, and P4) yielded interesting results. In comparison to the pure PSZ, the ceramic yields ranged between 5 and 15% and were increased in all cases, in correspondence with the content of hb-PolyFc. One possible reason for the higher yields could be the enhancement of the cross-linking reaction of hydrosilylation after the introduction of hb-PolyFc. Under this condition, the hyperbranched polymers are the cross-linked points with the cross-linked interface between PSZ and hb-PolyFc, as described in Figure 1. This is verified by the shift of DSC endothermic peaks to a low temperature as well as the decrease of the heat enthalpy for P2, P3, and P4 (Figure

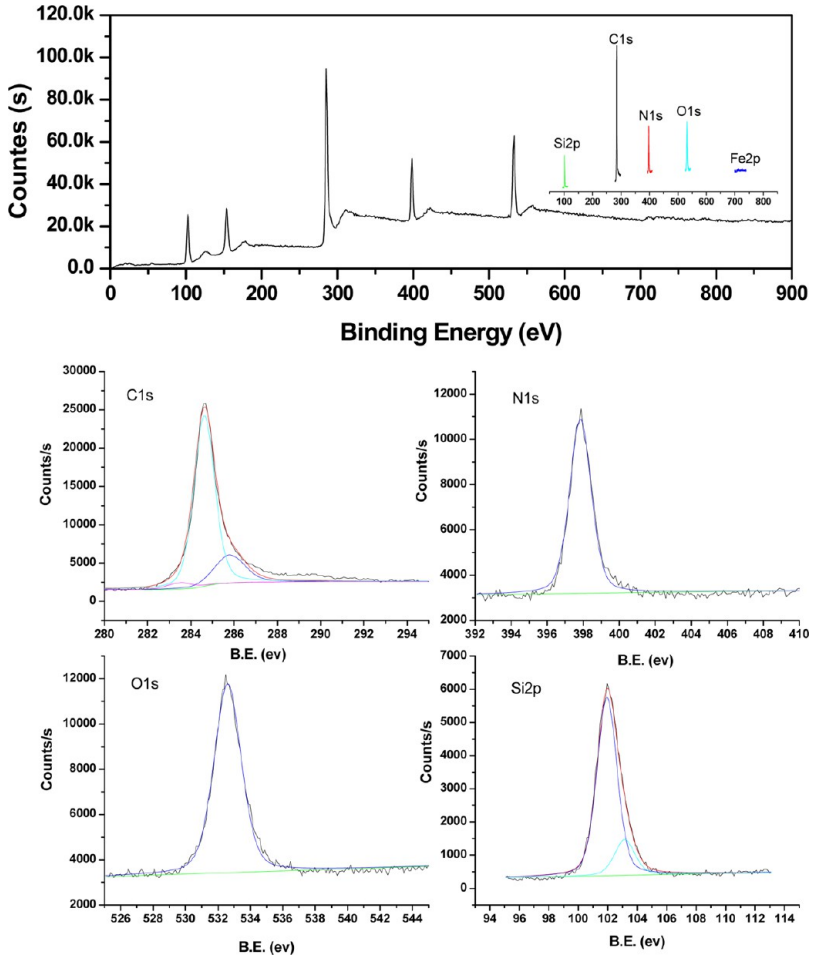

Figure 5. XPS spectra of a typical C4 ceramic.

2b). However, because of an increased thermolytic degradation of hb-PolyFc itself, as mentioned above, the increase in the ceramic yields of the mixed precursors, even with a high content of hb-PolyFc (15 or 33%), indicated that the pyrolysis of hb-PolyFc in the mixture was altered and that more elements were retained because of the deep cross-linking of the hydrosilylation, free-radical polymerization, or dehydrocoupling reaction. This can be further verified by the simultaneous mass spectrometry.

Figure 3 shows the analysis of simultaneous TGA and mass spectrometry, indicating the difference among the precursors of hb-PolyFc, PSZ, and their mixtures. A similar result has previously been reported by Riedel et al. with polysilazane.[28] The thermolysis of P1 is mainly accompanied with the evolution of H_2 (m/z = 2), hydrocarbons CH_x (x = 2−3, m/z = 14−15), CH_4 (m/z = 16), NH_3 (m/z = 17), and H_2O (m/z = 18) as well as oligomer fragments (m/z = 44−45). H_2O is released because of the oxidation of CH_4 and H_2 during pyrolysis. However, for P0, the evolution of H_2 (m/z = 2), hydrocarbons CH_x (x = 2−3, m/z = 14−15), CH_4 (m/z = 16), and oligomer fragments (m/z = 44) can be observed. For P1, the H_2 evolution starts at 350 °C as a result of the dehydrocoupling reactions of the Si−H/Si−H or Si−H/N−H groups, which are responsible for the decrease in weight over the wide temperature range between 300 and 950 °C. CH_4 or hydrocarbons are formed in the temperature range between 320 and 800 °C because of the decomposition of Si-CH_3 groups and the cleavage of C−C bonds. The NH_3 evolution (maximum at 450 °C) for P1 is in correspondence with transamination reactions, resulting in additional weight loss, which is not seen for P0.

However, the thermolysis of a mixture of PSZ and hb-PolyFc (i.e.,P2 and P3) is different from that of either PSZ or hb-PolyFc. First, the evolution of all of the hydrocarbons and CH_4 is delayed, and the decomposition is initiated at a higher temperature. Second, the evolution of gaseous NH_3 is reduced or cannot be observed during pyrolysis. Therefore, the decomposition of Si-CH_3 groups, the cleavage of C−C bonds, and the transamination reactions of polysilazane are reduced because of the incorporation of hb-PolyFc. Thus, the incorporation of a functional cross-linker of hyperbranched metallopolymer changes the pyrolysis behavior of a mixture (i.e., the delay of evolution of hydrocarbons), reducing the production of NH_3. The results further explain the enhanced ceramic yields for the mixture of PSZ or hb-PolyFc, as mentioned above.

3.2. Pyrolyzed Ceramics from Polymeric Precursors. After the pyrolysis of precursors of P1, P2, P3, and P4 under an argon atmosphere and high temperature, the bulk ceramic products were formed as C1, C2, C3, and C4, respectively (Figure 4a). The cross sections of resulting ceramics C2 and C3, formed from the precursors with a low content of hb-PolyFc, showed dense surfaces (Figures 4b,c and S4). For C4, obtained from the precursors with a high content of hb-PolyFc, uniform nanoscaled particles and clusters with dimensions of 20−40 nm were formed on the surfaces (Figure 4d). It should

be noted that several nanoscaled holes, which look like black particles (circle zone), were also observed because of the evolution of gas during ceramic formation. From the TEM morphology (Figures 4e,f), homogeneous nanostructures can be observed, which are different from the heterogeneous morphology with dispersed iron-based particle grains in the ceramic matrix prepared using inorganic compounds.[23,24]

The XPS and EDS analyses show the existence of silicon, iron, carbon, nitrogen, and oxygen elements in the ceramics (Figures 5 and S5). The atomic composition and ceramic formula for C0−C4 are described in Table 1. The ratio of iron/silicon for ceramics (C1−C4) is in the range of 1:100 to 6:100, as characterized by EDX. The ratio is in correspondence with the theoretical calculations from the composition of their polymeric precursors, as presented in Table 1. The detailed information on the ceramic components can be also derived from the XPS spectra (Figure 5), although the XPS in principle belongs to the surface analysis.[51] For C2−C4, the silicon nitrides (Si_3N_4) with a Si 2p bonding energy of 101.7 eV and N 1s bonding energy of 397.5 eV can be detected along with graphite carbon with a C 1s bonding energy of 284.7 eV. The silicon carbides (SiC) were also identified with a C 1s bonding energy of 282.7 eV. Besides the graphite-like carbon with a C 1s bonding energy of 284.7 eV, the carbon attached to oxygen via a single bond (B.E. = 286 eV in Figure 5a) can be found in C4, and the carbon attached to oxygen through a single bond (B.E. = 286 eV) and a double bond (B.E. = 288.2 eV) can be found in C1−C3, as shown in Figure S4. This type of carbon comes from the contamination from carbon dioxide on the sample surface before the XPS measurement.[52,53] Thus, the Si−Fe−C−N ceramics containing Si_3N_4, SiC crystals, and graphite carbons were formed after pyrolysis at 1100 °C.

The overall content of oxygen on the ceramic surface, as measured from XPS, is described in Table 1. It is derived from the oxygen absorption of ceramic powders before the measurement of XPS. However, Si_3N_4 is not completely resistant to oxidation. The surface of Si_3N_4 was therefore always slightly oxidized after contact with air, especially after the ceramics were milled.[54] As a result of a high concentration of silicon oxide on the surface, there are extra peaks at 103.15 and 530.2 eV in the Si2p spectrum (Figure 5), which corresponds to Si−O_x and Ni−Si−O compounds, respectively.[55]

3.3. XRD Analysis of Pyrolyzed Ceramics. The powder XRD patterns in Figure 6 further elucidate the fine-phase structures of pyrolyzed ceramics. For the precursor with a low content of hb-PolyFc (P2), ceramic C2 shows a near amorphous structure with a few silicon carbide (SiC) crystals and graphite carbons in comparison to the amorphous structure of C1 derived from P1. In C3 and C4, pyrolyzed from precursors with a high content of hb-PolyFc (P3 and P4), various crystals of α-silicon nitride (α-Si_3N_4), SiC, iron silicide (Fe_5Si_3), and graphite carbon were generated. The three peaks at 2θ = 40.8°, 45.2°, and 46.8° are indexed as the crystal face of the Fe_5Si_3 crystal [210], [211], and [300], respectively. The TEM images of dispersed ceramic C4 in Figure 4f illustrate the components of the crystals with clear lattice fringes. The measured d (211) spacing of 0.207 nm of Fe_5Si_3 agrees with the value of 0.20 nm calculated from XRD with a 2θ of 45.2°.[27] The existence of Fe_5Si_3 is also confirmed by the high-temperature DSC measurement of the C4 ceramics, as shown in Figure S6, where the endothermic peak at 1163 °C is attributed to the melting point of Fe_5Si_3.[56]

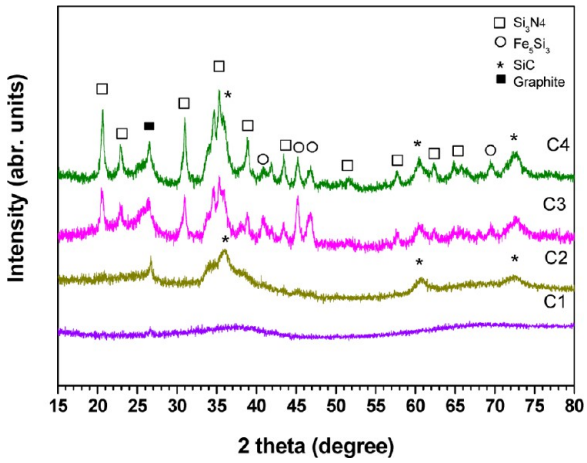

Figure 6. Powder XRD patterns of the Si−Fe−C−N multiphase ceramics with different iron contents (C2−C4) pyrolyzed at 1100 °C.

The results mentioned above indicate that the introduction of an appropriate amount of hb-PolyFc (more than 15%) promotes the formation of α-Si_3N_4 and SiC crystals. As has been reported,[57,58] metals such as iron, cobalt, or nickel may form a eutectic liquid with silicon, and the eutectic reaction can be initiated at a temperature lower than a pure metal and silicon system. Here, the iron atoms in hb-PolyFc react with the amorphous Si−C−N phase and form a eutectic liquid. Once the liquid phase is saturated, the solidification and formation of Fe_5Si_3 nuclei occurs and results in the formation of Fe_5Si_3, α-Si_3N_4, and SiC crystals. As a result, an exothermic peak centered at 1056 °C is observed in the DSC thermograms (Figure 2b). In other words, iron atoms from hb-PolyFc react with the amorphous Si−C−N phase to promote the formation of either α-Si_3N_4 or SiC crystals.

Different from the formation of the Fe_3Si crystals in an iron-powder-modified PSZ system at 1100 °C[56] and the Fe_3C crystals in ferrocene-modified PSZ hexamethyldisilazane at 1200 °C,[59] the uniform iron atoms from soluble hb-PolyFc in PSZ are helpful in the formation of metastable Fe_5Si_3 crystals and stable α-Si_3N_4, SiC crystals at a relatively low pyrolysis temperature. After high-temperature annealing, the metastable Fe_5Si_3 phase further transforms into the stable Fe_3Si phase, which is proved by the XRD patterns in Figure 7. For the C2 or C4 annealed ceramics at 1300 °C, the two peaks at 2θ = 40.8°

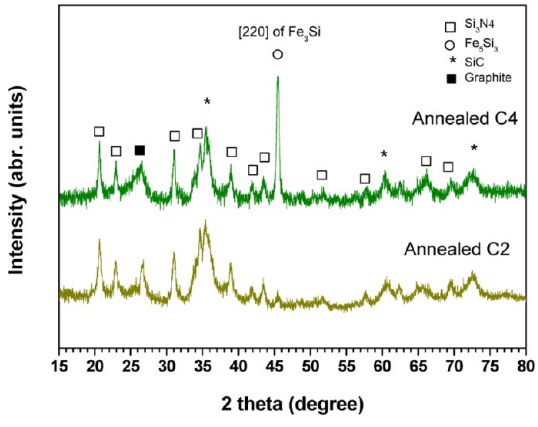

Figure 7. Powder XRD patterns of the Si−Fe−C−N multiphase ceramics (C2, C4) annealed at 1300 °C (Ar/h).

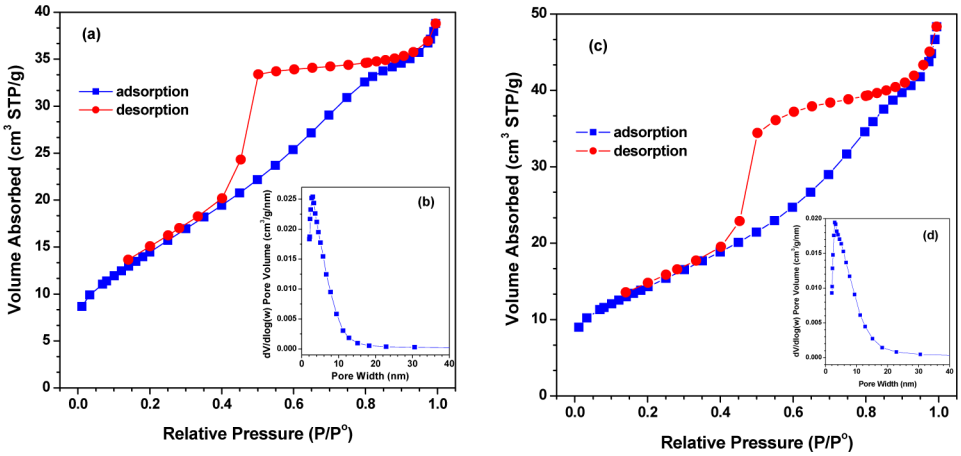

Figure 8. Nitrogen adsorption−desorption isotherm and the corresponding pore-size distribution (PSD) calculated using the adsorption branch of the BJH algorithm for ceramic C3 (a, b) and C4 (c, d).

and 46.8°, indexed as the [210] and [300] crystal face of Fe_5Si_3 crystals, disappear. The intensity of the sharp peak at $2\theta = 45.5°$ was enhanced and indexed as the [220] crystal face of the Fe_3Si crystal (ICDD data file 73-1703). The transformation can be verified by the high-temperature DSC analysis in Figure S6, where a higher endothermic peak centered at 1186 °C is observed and is indexed as the melting point of Fe_3Si in the annealed C4. As a comparison, the endothermic peak at 1163 °C corresponds to the melting point of Fe_5Si_3 in the original C4. From the analysis mentioned above, α-Si_3N_4, SiC, and Fe_5Si_3 nanocrystal-containing ceramics were formed via bulk pyrolysis of the precursors with a high content of hb-PolyFc at 1100 °C. After annealing at 1300 °C, a stable Fe_3Si nanocrystal was formed after the transformation of Fe_5Si_3.

3.4. Nitrogen Adsorption of Ceramics. The nitrogen physisorption isotherms for representative ceramics C3 and C4 are presented in Figure 8. The typical IV isotherms reveal capillary condensation accompanied with a wide nitrogen adsorption−desorption hysteresis loop, which is the typical characteristic for mesoporous materials. The wide hysteresis loops in a N_2 atmosphere suggest a delay in both the evaporation and condensation, which can be also observed in the pores with narrow necks and wider bodies (ink-bottle pores).[60,61] The mesopore size distributions can be calculated by applying the nitrogen metastable adsorption branch kernels (Table 2). The specific surface area for C3 and C4 is in the range of 51−54 m^2/g, much lower than that observed for the typical porous ceramic materials.[28] In contrast, for C2, obtained from the precursor with a low content of hb-PolyFc (5 wt %), the nitrogen physisorption isotherm in Figure S7b shows a dense ceramic structure. Therefore, the pyrolysis of the polymeric precursors PSZ and hb-PolyFc generated dense ceramics with low specific surface area.

Table 2. Specific Surface Area, Pore Volume, and Average Pore Width of Ceramics Pyrolyzed at 1100 °C

sample	content of hb-PolyFc (wt %)	specific surface area (m^2/g)[a]	pore volume (cm^3/g)[b]	average pore width (nm)
C3	15	53.46	0.05678	4.25
C4	33	51.52	0.06768	5.25

[a]The BET equivalent specific surface area was calculated by the Brunauer−Emmett−Teller (BET) method. [b]The pore-size distribution was calculated by the quenched solid density functional theory (QSDFT) method.

3.5. Magnetic Property of Nanocrystal-Containing Ceramics. A superconducting quantum interference device (SQUID) was employed to monitor the magnetization curves of ceramics at a temperature of 300 K. The magnetization curves for representative ceramics (C2−C4) are shown in Figure 9. In the magnetic field at a temperature of 300 K,

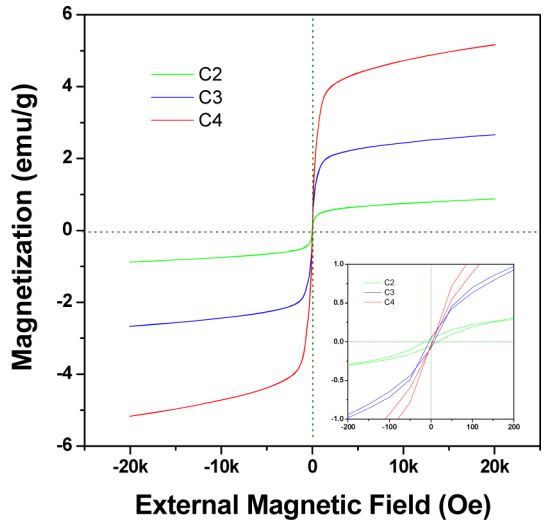

Figure 9. Plots of magnetization, M, versus the external applied magnetic field, H, at 300 K for Si−Fe−C−N ceramics with different iron contents (C2−C4) (inset: enlarged portion of the plots at the low H).

sample C4 was swiftly magnetized with an immediate rise in its magnetization curve. As shown in the enlarged magnetization curves in the low-field region, an ultralow hysteresis loop can be identified with a remanence (M_r) of 0.04 emu/g and a coercivity (H_c) of 5 Oe. The low hysteresis loops indicate the excellent ferromagnetic property of C4. After annealing at 1300 °C, a decrease of M_s was observed for C4 and C2, as presented in Figures 10 and S8. The first reason for a decrease in M_s is the formation of Fe_3Si crystals with a low M_r. The second reason might be the generation of some oxides, which are difficult to avoid during high-temperature annealing, even in an argon atmosphere.

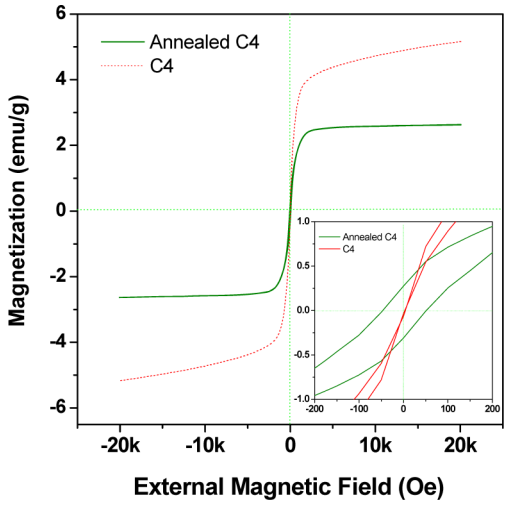

Figure 10. Plots of magnetization, *M*, versus the external applied magnetic field, *H*, at 300 K for C4 after annealing at 1300 °C.

The saturation magnetization of ceramics was found to be dependent on the content of hp-PolyFc in the precursors employed (i.e., the content of iron in the matrix), as shown in Table 1. The saturation magnetization (M_s) for C4 was determined to be 5.16 emu/g at 300 K. For C2 and C3 (from precursors with low content of hb-PolyFc), the lower M_s of 2.8 and 0.8 emu/g in comparison to that of C4 is attributed to the low content of iron silicide in the ceramic matrix.

However, for all ceramics C2−C4, M_s is far lower than the pure iron silicide nanoparticles synthesized using a high-temperature reduction method.[62] The main reason for this is the presence of the nonmagnetic and amorphous phases in ceramics detected by XRD. Additionally, the surface spins at the interface between the magnetic components and nonmagnetic surroundings in ceramics can reduce the total magnetic moments, resulting in a decrease in the magnetization.[38,63,64] However, the ultralow hysteresis loop for all of the ceramics, including C2, C3, and C4, can be observed (i.e., both low remanence (M_r = 0.04 emu/g) and low coercivity (H_c = 5 Oe)). The structure analyses presented above reveals that the major components of magnetic phases in C2−C4 are iron silicide nanocrystals, which may be the reason for the near-0 M_r and H_c values.

4. CONCLUSIONS

Nanocrystal-containing magnetoceramics were synthesized by bulk pyrolysis of hb-PolyFc terminated with silicon hydrogen bonds as a functional cross-linker for commercial linear PSZ. During the pyrolysis, the evolution of hydrocarbons and NH_3 were delayed and more elements were retained. As a result, the hb-PolyFc significantly enhanced the ceramic yields from a mixture of precursors because of the deep cross-linking from the hydrosilylation reaction between hb-PolyFc and PSZ as well as with the hydrosilylation reaction, the radical polymerization of double bonds, and the dehydrocoupling reaction of PSZ. The formation of α-Si_3N_4 and SiC crystals is promoted by the nucleation of Fe_5Si_3 from the reaction of iron atoms with the amorphous SiCN phase. After annealing at 1300 °C, stable Fe_3Si nanocrystals are formed from the transformation of the Fe_5Si_3 phase. The ceramics containing iron silicide nanocrystals show good ferromagnetism with an ultralow hysteresis loss (near 0). Different from the heterogeneous morphology with dispersed metal-based particle grains from insoluble inorganic metal compounds or complex coordination compounds, the usage of a soluble hyperbranched metallopolymer offers a convenient synthesis strategy for the synthesis of tunable magnetoceramics with a homogeneous nanostructure. These functional nanostructured ceramics could have the potential for practical applications in electromagnetic systems, information storage, and magnetic refrigeration.

■ ASSOCIATED CONTENT

Ⓢ Supporting Information

NMR spectra, GPC traces, XPS spectra, and high-temperature DSC results of polymers and ceramics. This material is available free of charge via the Internet at http://pubs.acs.org.

■ AUTHOR INFORMATION

Corresponding Author

*E-mail: kongjie@nwpu.edu.cn. Tel.: +86-29-88431621. Fax: +86-29-88431621.

Notes

The authors declare no competing financial interest.

■ ACKNOWLEDGMENTS

This research is supported by the Natural Science Foundation of China under grant no. 21174112. J.K. acknowledges the support from the Program for New Century Excellent Talents of the Education Ministry of China (NCET-11-0817) and the Basic Scientific Research Foundation of Northwestern Polytechnical University. The help of Dr. G. Motz (CME, Universität Bayreuth) for the discussion is gratefully acknowledged.

■ REFERENCES

(1) Colombo, P.; Mera, G.; Riedel, R.; Sorarù, G. D. *J. Am. Ceram. Soc.* **2010**, *93*, 1805−1837.
(2) Wideman, T.; Sneddon, L. G. *Chem. Mater.* **1996**, *8*, 3−5.
(3) Bernard, S.; Weinmann, M.; Cornu, D.; Miele, P.; Aldinger, F. *J. Eur. Ceram. Soc.* **2005**, *25*, 251−256.
(4) Bhandavat, R.; Kuhn, W.; Mansfield, E.; Lehman, J.; Singh, G. *ACS Appl. Mater. Interfaces* **2012**, *4*, 11−16.
(5) Sarkar, S.; Zou, J. H.; Liu, J. H.; Xu, C. Y.; An, L. N.; Zhai, L. *ACS Appl. Mater. Interfaces* **2010**, *2*, 1150−1156.
(6) Guron, M. M.; Wei, X. L.; Welna, D.; Krogman, N.; Kim, M. J.; Allcock, H.; Sneddon, L. G. *Chem. Mater.* **2009**, *21*, 1708−1715.
(7) Wilson, A. M.; Zank, G.; Eguchi, K.; Xing, W.; Yates, B.; Dahn, J. R. *Chem. Mater.* **1997**, *9*, 2139−2144.
(8) Iwamoto, Y.; Sato, K.; Kato, T.; Inada, T.; Kubo, Y. *J. Eur. Ceram. Soc.* **2005**, *25*, 257−264.
(9) Colombo, P. *J. Eur. Ceram. Soc.* **2008**, *28*, 1389−1395.
(10) Günthner, M.; Kraus, T.; Dierdorf, A.; Decker, D.; Krenkel, W.; Motz, G. *J. Eur. Ceram. Soc.* **2009**, *10*, 2061−2068.
(11) Schulz, M. *Adv. Appl. Ceram.* **2009**, *108*, 454−460.
(12) Liew, L. A.; Zhang, W. G.; An, L. N.; Shah, S.; Luo, R. L.; Liu, Y. P.; Cross, T.; Dunn, M. L.; Bright, V.; Daily, J. W.; Raj, R.; Anseth, K. *Am. Ceram. Soc. Bull.* **2001**, *80*, 25−30.
(13) Liew, L. A.; Liu, Y. P.; Luo, R. L.; Cross, T.; An, L. N.; Bright, V. M.; Dunn, M. L.; Daily, J. W.; Raj, R. *Sens. Actuators, A* **2002**, *95*, 120−134.
(14) Graczyk-Zajac, M.; Mera, G.; Kaspar, J.; Riedel, R. *J. Eur. Ceram. Soc.* **2010**, *30*, 3235−3243.
(15) Bhandavat, R.; Singh, G. *ACS Appl. Mater. Interfaces* **2012**, *4*, 5092−5097.
(16) Bhandavat, R.; Singh, G. *J. Phys. Chem. C* **2013**, *117*, 11899−11905.

(17) Mitomo, M.; Kim, Y. W.; Hirotsuru, H. *J. Mater. Res.* **1996**, *11*, 1601−1604.
(18) Shinoda, Y.; Nagano, T.; Wakai, F. *J. Am. Ceram. Soc.* **1999**, *82*, 771−773.
(19) Yamamoto, T.; Kitaura, H.; Kodera, Y.; Ishii, T.; Ohyanagi, M.; Muir, Z. A. *J. Am. Ceram. Soc.* **2004**, *87*, 1436−1441.
(20) Hauser, R.; Francis, A.; Theissmann, R.; Riedel, R. *J. Mater. Sci.* **2008**, *43*, 4042−4049.
(21) Saha, A.; Shah, S. R.; Raj, R.; Russek, S. E. *J. Mater. Res.* **2003**, *18*, 2549−2551.
(22) Yang, W.; Miao, H.; Xie, Z.; Zhang, L.; An, L. N. *Chem. Phys. Lett.* **2004**, *383*, 441−444.
(23) Park, J. H.; Park, K. H.; Kim, D. P. *J. Ind. Eng. Chem.* **2007**, *13*, 27−32.
(24) Yu, Y. X.; An, L. N.; Chen, Y. H.; Yang, D. X. *J. Am. Ceram. Soc.* **2010**, *93*, 3324−3329.
(25) Dumitru, A.; Stamatin, I.; Morozan, A.; Mirea, C.; Ciupina, V. *Mater. Sci. Eng., C* **2007**, *27*, 1331−1337.
(26) (a) Zaheer, M.; Schmalz, T.; Motz, G.; Kempe, R. *Chem. Soc. Rev.* **2012**, *41*, 5102−5116.
(27) Hojamberdiev, M.; Prasad, R. M.; Fasel, C.; Riedel, R.; Ionescu, E. *J. Eur. Ceram. Soc.* **2013**, *33*, 2465−2472.
(28) Bazarjani, M. S.; Kleebe, H. -J.; Mueller, M. M.; Fasel, C.; Yazdi, M. B.; Gurlo, A.; Riedel, R. *Chem. Mater.* **2011**, *23*, 4112−4123.
(29) Zaheer, M.; Keenan, C. D.; Hermannsdörfer, J.; Roessler, E.; Motz, G.; Senker, J.; Kempe, R. *Chem. Mater.* **2012**, *24*, 3952−3963.
(30) Glatz, G.; Schmalz, T.; Kraus, T.; Haarmann, F.; Motz, G.; Kempe, R. *Chem.—Eur. J.* **2010**, *16*, 4231−4238.
(31) Foucher, D. A.; Tang, B. Z.; Manners, I. *J. Am. Chem. Soc.* **1992**, *114*, 6246−6248.
(32) Tang, B. Z.; Petersen, R.; Foucher, D. A.; Lough, A.; Coombs, N.; Sodhib, R.; Manners, I. *J. Chem. Soc., Chem. Commun.* **1993**, 523−525.
(33) Whittell, G. R.; Manners, I. *Adv. Mater.* **2007**, *19*, 3439−3468.
(34) Maclachlan, M. J.; Ginzburg, M.; Coombs, N.; Coyle, T. M.; Raju, N. P.; Greedan, J. E.; Ozin, G. A.; Manners, I. *Science* **2000**, *287*, 1460−1463.
(35) Nguyen, P.; Gómez-Elipe, P.; Manners, I. *Chem. Rev.* **1999**, *99*, 1515−1548.
(36) Chen, H.; Kong, J.; Tian, W.; Fan, X. D. *Macromolecules* **2012**, *45*, 6185−6195.
(37) Kumar, M.; Pannell, K. H. *J. Inorg. Organomet. Polym.* **2008**, *18*, 131−142.
(38) Sun, Q. H.; Lam, J. W. Y.; Xu, K. T.; Xu, H. Y.; Cha, J. A. K.; Wong, P. C. L.; Wen, G. H.; Zhang, X. X.; Jing, X. B.; Wang, F. S.; Tang, B. Z. *Chem. Mater.* **2000**, *12*, 2617−2614.
(39) Sun, Q. H.; Xu, K. T.; Peng, H.; Zheng, R. H.; Haussler, M.; Tang, B. Z. *Macromolecules* **2003**, *36*, 2309−2320.
(40) Shi, J. B.; Tong, B.; Li, Z.; Shen, J. B.; Zhao, W.; Fu, H. H.; Zhi, J. G.; Dong, Y. P.; Häussler, M.; Lam, J. W. Y.; Tang, B. Z. *Macromolecules* **2007**, *40*, 8195−8204.
(41) Kulbaba, K.; Cheng, A.; Bartole, A.; Greenberg, S.; Resendes, R.; Coombs, N.; Safa-Sefat, A.; Greedan, J. E.; Stöver, H. D. H.; Ozin, G. A.; Manners, I. *J. Am. Chem. Soc.* **2002**, *124*, 12522−12534.
(42) Wang, X. S.; Guerin, G.; Wang, H.; Wang, Y. S.; Manners, I.; Winnik, M. A. *Science* **2007**, *317*, 644−647.
(43) Rider, D. A.; Liu, K.; Eloi, J. C.; Vanderark, L.; Yang, L.; Wang, J. Y.; Grozea, D.; Lu, Z. H.; Russell, T. P.; Manners, I. *ACS Nano* **2008**, *2*, 263−270.
(44) Wurm, F.; Hilf, S.; Frey, H. *Chem.—Eur. J.* **2009**, *15*, 9068−9077.
(45) Kong, J.; Schmalz, T.; Motz, G.; Müller, A. H. E. *Macromolecules* **2011**, *44*, 1280−1291.
(46) Wang, S. J.; Fan, X. D.; Kong, J.; Wang, X.; Liu, Y. Y.; Zhang, G. B. *J. Polym. Sci., Part A: Polym. Chem.* **2008**, *46*, 2708−2720.
(47) Wang, S. J.; Fan, X. D.; Kong, J.; Lu, J. R. *Polymer* **2009**, *50*, 3587−3594.
(48) Kong, J.; Schmalz, T.; Motz, G.; Müller, A. H. E. *J. Mater. Chem. C* **2013**, *1*, 1507−1514.
(49) Ischenko, V.; Pippel, E.; Woltersdorf, J.; Yappi, B. R. N.; Hauser, R.; Fasel, C.; Riedel, R.; Poli, F.; Müller, K. *Chem. Mater.* **2008**, *20*, 7148−7156.
(50) Jain, R.; Choi, H.; Lalancette, R. A.; Sheridan, J. B. *Organomettallics* **2005**, *24*, 1468−1476.
(51) McIntyre, N. S.; Zetaruk, D. G. *Anal. Chem.* **1977**, *49*, 1521−1529.
(52) Huntley, D. R. *J. Phys. Chem.* **1992**, *96*, 4550−4558.
(53) Rufael, T. S.; Huntley, D. R.; Mullins, D. R.; Gland, J. L. *J. Phys. Chem. B* **1998**, *102*, 3431−3440.
(54) Finster, J.; Heeg, J.; Klinkenberg, E.-D. *Prog. Surf. Sci.* **1990**, *35*, 179−184.
(55) Saha, S. K.; Howell, R. S.; Hatalis, M. K. *Thin Solid Films* **1999**, *347*, 278−283.
(56) Francis, A.; Ionescu, E.; Fasel, C.; Riedel, R. *Inorg. Chem.* **2009**, *48*, 10078−10083.
(57) Pan, Y.; Baptista, J. L. *J. Am. Chem. Soc.* **2002**, *124*, 12522−12534.
(58) Mitomo, M. *J. Mater. Sci.* **1977**, *12*, 273−276.
(59) Dumitru, A.; Ciupina, V.; Stamatin, I.; Prodan, G.; Morozan, A.; Mirea, C. *J. Optoelectron. Adv. Mater.* **2006**, *8*, 50−54.
(60) (a) Yu, J. G.; Yu, J. C.; Ho, W. K.; Leung, M. K. P.; Cheng, B.; Zhang, G. K.; Zhao, X. J. *Appl. Catal., A* **2003**, *255*, 309−320.
(61) Yu, J. G.; Yu, J. C.; Cheng, B.; Hark, S. K.; Iu, K. *J. Solid State Chem.* **2003**, *174*, 372−380.
(62) Dahal, N.; Chikan, V. *Chem. Mater.* **2010**, *22*, 2892−2897.
(63) Liu, G. J.; Ding, J. F.; Hashimoto, T.; Kimishima, K.; Winnik, F. M.; Nigam, S. *Chem. Mater.* **1999**, *11*, 2233−2240.
(64) Zhang, L.; Papaefthymiou, G. C.; Ying, J. Y. *J. Appl. Phys.* **1997**, *81*, 6892−6900.